Preparation of magnetically recoverable bentonite–Fe3O4–MnO2 composite particles for Cd(II) removal from aqueous solutions

Jiang, Liying; Ye, Qichao; Chen, Jianmeng; Chen, Zhong; Gu, Youli

2017

Jiang, L., Ye, Q., Chen, J., Chen, Z., & Gu, Y. (2018). Preparation of magnetically recoverable bentonite–Fe3O4–MnO2 composite particles for Cd(II) removal from aqueous solutions. Journal of Colloid and Interface Science, 513, 748-759.

https://hdl.handle.net/10356/89359

https://doi.org/10.1016/j.jcis.2017.11.063

Preparation of magnetically recoverable bentonite-Fe_3O_4-MnO_2 composite particles for Cd(II) removal from aqueous solutions

Liying Jiang[1]*, Qichao Ye[1], Jianmeng Chen[1], Zhong Chen*[2], Youli Gu[1], Xiang Cao[1]

1. College of Environment, Zhejiang University of Technology, Hangzhou 310032, China
2. School of Materials Science and Engineering, Nanyang Technological University, 50 Nanyang Avenue, Singapore 639798, Singapore

Corresponding authors

*College of Environment, Zhejiang University of Technology, Hangzhou 310032, China

E-mail: jiangly@zjut.edu.cn

Phone: +86-571-88320365

Fax: +86-571-88320882

* School of Materials Science and Engineering, Nanyang Technological University, 50 Nanyang Avenue, Singapore 639798, Singapore

E-mail: aszchen@ntu.edu.sg

Phone: +65-67904256

Fax: +65-67906727

Highlights

- A novel bentonite-Fe_3O_4-MnO_2 absorbent was prepared via a co-precipitation process
- The MnO_2 coating has greatly improved Cd(Ⅱ) removal capacity
- The kinetic and isothermal data fit well with the pseudo-second-order and the Freundlich models, respectively
- Hydroxyl group played an important role in Cd(Ⅱ) adsorption process

Graphical Abstract

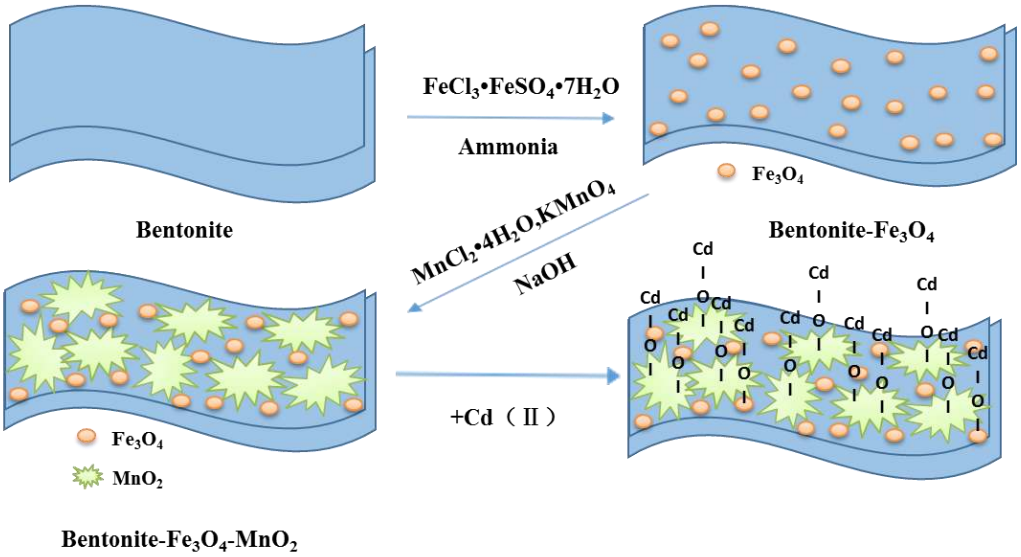

Abstract

In the present study, the bentonite-Fe_3O_4-MnO_2 composite was synthesized by combining bentonite with Fe_3O_4 and MnO_2 through co-precipitation. The magnetic properties, morphology and structure of the composites were characterized by vibrating sample magnetometer (VSM), scanning electron microscopy (SEM) and transmission electron microscopy (TEM). The obtained bentonite-Fe_3O_4-MnO_2 consists of Fe_3O_4 nanoparticles orderly assembled on the surface of bentonite and MnO_2 sheets coated as an outer layer. The resulting composite particles possess a saturation magnetization of 13.4-30.5 emu/g and high specific surface area of 796.99 m^2/g. The adsorption behaviors of bentonite-Fe_3O_4-MnO_2 for Cd(II) removal were evaluated by batch equilibrium experiments. The kinetic and isothermal data are well fitted with the pseudo-second-order model and the Freundlich model, respectively. The adsorption reached equilibrium within 30 min and the Freundlich capacities of bentonite-Fe_3O_4-MnO_2 was 35.35 mg/g. The adsorption capacity of Cd(II) increased with an increasing pH and was also dependent on the ionic strength. FTIR and XPS analysis implied the combination of the surface hydroxyl groups of bentonite-Fe_3O_4-MnO_2 and the Cd(II) in the solution. Moreover, the prepared bentonite-Fe_3O_4-MnO_2 can be easily recycled taking advantage of the magnetic properties and reused. The results proved that the designed bentonite-Fe_3O_4-MnO_2 absorbent is a promising material for the treatment of Cd contaminated water.

1. Introduction

Heavy metal pollution has become a serious environmental problem due to its non-biodegradability, bioaccumulation and high toxicity [1-2]. Cadmium is one of the most harmful heavy metals to human for its high toxicity even at low concentrations. It has been reported that chronic exposure to Cd(II) could cause renal disturbances, lung cancer, bone lesions, prostatic proliferative lesions, and hypertension [3-4]. World Health Organization (WHO) has set the cadmium standard for drinking water to a level less than 5 μg/L. Hence, it is essential to explore effective, reliable and cost-effective techniques for Cd(II) removal prior to its solution being allowed to be released to the environment. Adsorption is considered one of the most promising and widely adopted approaches to remove heavy metals owing to its simplicity of application, economic viability, environment-friendliness, ability to be regenerated, and high efficiency [5-6]. For this purpose, developing adsorbents with high adsorption capacity and stable treatment efficiency is of critical importance.

Raw bentonite is a common type of clay minerals on the earth, and has been widely used for removing heavy metal ions because of its high specific surface areas, low-cost, great abundance, chemical and mechanical stability, relatively high cation exchange capacity (CEC) and good adsorption capability [7-12]. However, the difficulty to separate bentonite from water limits its practical application. In recent years, magnetic materials (such as Fe_3O_4) that can be easily separated from solution using an external magnetic field have been extensively studied for water treatment [13-16]. Therefore, it can be expected that the combination of bentonite and Fe_3O_4 not only brings about a magnetic hybrid with high adsorption capacity, but also overcomes some drawbacks of

Fe_3O_4, which includes agglomeration and chemical instability in acidic media [17]. Fe_3O_4 alone is not able to efficiently remove the contaminants because of its smaller adsorption ability and lower bonding affinity in comparison with hydrated ferric oxide [18].

Manganese oxides (MnO_2) are low cost, environmentally friendly metal oxides and omnipresent in the natural environment. They have strong oxidizing/adsorptive abilities due to their large specific surface areas [19-21]. Several researches reported that MnO_2 attenuates numerous heavy metal ions via adsorption, ion-exchange, or coprecipitation [22-23]. It has been reported that the modification of the Fe_3O_4 surface with MnO_2 can increase the removal efficiency of the magnetic nanoparticles for heavy metal ions [24-26]. Kim et al. synthesized a MnO_2-coated magnetic nanocomposite (Fe_3O_4/MnO_2) by a mild hydrothermal process and proved that it exhibited a greatly improved removal capacity toward four different heavy metals compared to unmodified Fe_3O_4 nanoparticles [25]. A nanocomposites of Fe_3O_4-reduced graphite oxide-MnO_2 were synthesized by Luo et al. combined the oxidation property of manganese dioxide, the high surface area of GO and magnetic features of Fe_3O_4, which had a high removal capacity towards both As(Ⅴ) and As(Ⅲ) [27].

Based on our previous research about preparation of MnO_2-coated diatomite adsorbent [28], loading the manganese oxide on the surface of magnetic bentonite (bentonite-Fe_3O_4) is anticipated to increase the removal capacity of magnetic bentonite while making the composite easily recyclable. Therefore, the main objectives of this study are to synthesize a novel magnetic bentonite coated with manganese oxide, and to

characterize the adsorbent using a variety of techniques. The adsorption ability for Cd(Ⅱ) will be investigated with a focus on the effect of contact time, pH and ionic strength on Cd(II) sorption. The adsorption kinetics and adsorption isotherms will be measured and the sorption mechanism discussed. The regeneration and reusability of the composite adsorbent will also be demonstrated.

2. Materials and methods

2.1. Materials

The bentonite used for this study was purchased from Sigma-Aldrich (St. Louis, MO, USA). Ferric chloride ($FeCl_3$), ferrous sulfate heptahydrate ($FeSO_4 \cdot 7H_2O$), ammonia (NH_4OH, 25-28%), manganese chloride tetrahydrate ($MnCl_2 \cdot 4H_2O$), potassium permanganate ($KMnO_4$), sodium hydroxide (NaOH) , concentrated nitric acid (HNO_3, 65-68%), sodium chloride (NaCl), cadmium nitrate tetrahydrate ($Cd(NO_3)_2 \cdot 4H_2O$) were purchased from Shanghai Zhenxin Reagent Co. Ltd (China). Cadmium nitrate tetrahydrate ($Cd(NO_3)_2 \cdot 4H_2O$, purity > 99%) was purchased from Shanghai Aladdin Chemical Co. Ltd (China). All the chemicals are analytical reagent (AR) grade without further purification. Water used was distilled and purified by a Milli-Q system.

Cd(II) stock solutions (1000 mg/L) were prepared by $Cd(NO_3)_2 \cdot 4H_2O$ in purified water. Fresh initial solutions of varying Cd(II) concentrations were prepared daily by diluting the stock solution with ultrapure water.

2.2 Preparation of bentonite-Fe_3O_4-MnO_2

The bentonite-Fe_3O_4-MnO_2 nanocomposite was synthesized via a two-step co-

precipitation process according to the previous literatures [29-30].

First, 2.821 g of bentonite was added into a 500 mL three-neck round flask containing 300 mL solution of $FeCl_3$ (3.952 g), and continuously stirred for 4 h. Then the solution was purged with N_2 for about half an hour followed by the quickly addition of 3.387 g $FeSO_4 \cdot 7H_2O$ to the flask. The solution was heated to 90 ℃ in N_2 atmosphere and a certain amount of ammonia was added with vigorous agitation. Afterwards, the obtained black suspension was kept stirring for another 1 h at 90 °C and then cooled to room temperature. The fabricated bentonite-Fe_3O_4 was separated by a magnet and washed with ultrapure water repeatedly until the conductivity was < 2 μs/cm. At last, the bentonite-Fe_3O_4 was dried at a vacuum freeze drying apparatus. The dry material was crushed and stored in a desiccator.

To select appropriate content of loading MnO_2 on the bentonite-Fe_3O_4, different molar ratios (2:1, 1:1, 1:1.5, 1:2) of Fe to Mn were prepared and denoted as bentonite-Fe_3O_4-MnO_2 (2:1), bentonite-Fe_3O_4-MnO_2 (1:1), bentonite-Fe_3O_4-MnO_2 (1:1.5), and bentonite-Fe_3O_4-MnO_2 (1:2), respectively. They were prepared as follows [30]: 1 g bentonite-Fe_3O_4 composite was dispersed in a three-neck round flasks (500 mL) containing 200 mL ultrapure water under N_2 flow. Different amount of $MnCl_2 \cdot 4H_2O$ was added into the suspension under stirring. After 4 h mixing, the suspensions were heated to 80 ℃ and added with the solutions containing corresponding amounts of $KMnO_4$ and NaOH dropwise, followed by a continuous agitation for another 2 h. Afterwards, the dark-brown precipitate was separated by magnetic attraction and rinsed repeatedly with ultrapure water until the conductivity was < 2 μs/cm. Finally, the

product was dried in a vacuum freeze drying apparatus. The dry material (denoted as bentonite-Fe_3O_4-MnO_2) was ground and stored in a desiccator.

2.3 Characterization

The magnetic property of adsorbents was analyzed by a VSM (Meghnatis Daghigh Kavir Co., Kashan, Iran). The surface morphologies and elemental compositions of the absorbents were analyzed with Quanta F250 SEM-EDX (FEI, USA) and Hitachi HT−7700 TEM (Hitachi, Japan) operating at 100 kV. The specific surface areas were measured by nitrogen adsorption/desorption analysis using the BET method with a Micromeritics ASAP 2010 surface area analyzer (Norcross, GA, USA). XRD analysis was carried out on an X'Pert PRO diffractometer (PANalytical Co., Almelo, The Netherlands) using Cu Kα (λ = 0.154 nm) and operating at 40 kV and 30 mA. The powder diffraction pattern was obtained in a scanning mode with a 0.02 (2θ) step size from 10 to 80° at 4° per min. FTIR spectra from 400 to 4000 cm^{-1} were collected using a Nicolet 6700 FTIR spectrophotometer Spectrum (Thermo, USA) to identify functional groups on the adsorbent surface. XPS data were collected on a Kratos AXIS Ultra DLD spectrometer with monochromatic Al Kα radiation. The zeta potential was measured by a Zetasizer 2000 (Malvern Co., UK). Aqueous sample suspension was dispersed using an ultrasonic bath and an average of three measurements was taken to represent the measured potential.

In addition, the leaching of iron or manganese at different pH (3.0-10.0) was examined for evaluating the absorbent stability. 0.3g of bentonite-Fe_3O_4-MnO_2 adsorbents (1:1.5)

was added into 100 mL of 100 mg/L Cd(II) solution and stirred at 160 rpm under 25 °C for 24 h.

2.4 Bath adsorption experiments

In a typical reaction, adsorption experiment was conducted in a 250 mL conical flask at 25 °C and pH 6.0 (adjusted by 0.1 M HNO_3 or NaOH). 0.3 g of sorbent was added to 10 mL Cd(II) solution with a concentration of 100 mg/L. The mixture was stirred thoroughly at 160 rpm, then the sample solution was separated by a magnet.

To determine the optimal Fe/Mn ratio, bentonite-Fe_3O_4-MnO_2 adsorbents with different Fe/Mn ratio (2:1, 1:1, 1:1.5 and 1:2) were added to the Cd(II) solution for 24 h. Combined the Cd(II) removal efficiency with the saturation magnetization values, the optimal MnO_2 loading on bentonite-Fe_3O_4-MnO_2 was selected for the subsequent experiment.

For the kinetic experiment, adsorbents (bentonite, bentonite-Fe_3O_4, or bentonite-Fe_3O_4-MnO_2 (1:1.5)) and 100 mL of 100 mg/L Cd(II) solution were used, and the stirred time intervals were controlled from 1 to 1440 min. The adsorption isotherms was established on 0.3 g bentonite-Fe_3O_4-MnO_2 (1:1.5) adsorbents with initial concentration of Cd(II) from 50 to 400 mg/L for 24 h.

To investigate the effects of pH on the sorption of Cd(II), the adsorption experiment was tested on 0.3 g adsorbent with initial concentration of 100 mg/L Cd(II) by varying the initial solution pH from 2.0 to 9.0. In the ionic strength effect study, NaCl with different concentrations (0, 0.001, 0.01, 0.1, 0.2 M) were used as electrolyte

background with 0.3 g adsorbents and initial concentration of Cd(II) at 100 mg/L. The adsorption capability for trace Cd(II) on bentonite-Fe_3O_4-MnO_2(1:1.5) was also studied by adding different amounts (0.01-0.06 g/L) of adsorbents into a series of 100 mL Cd(II) solution at 100 μg/L concentration.

For the reusability of bentonite-Fe_3O_4-MnO_2 (1:1.5) after adsorption, 0.1 mol/L HNO_3 solution (pH = 3) was chosen as the desorption solution. The mixture was shaken vigorously at 25 °C for 24 h, and then separated from the suspension by a magnet. The separated samples were suspended in HNO_3 solution with stirring for 4 h, washed with ultrapure water to neutral pH and freeze-dried before re-adsorption in the next cycle. The adsorption / desorption experiment was repeated 5 times.

Sample solutions after separation were filtered using 0.22-μm PTFE syringe filters and the concentration of Cd(II) in the supernatant was determined by an atomic absorption spectrophotometer (Analyst 800, Perkin Elmer Co., Norwalk, CT, USA). All experiments were conducted in triplicate, and the data shown were the average values.

Sorption capacity was calculated using Eqs. (1) and (2):

$$q_t = \frac{V(C_0 - C_t)}{m} \quad (1)$$

$$\text{removal efficiency } (\%) = \frac{(C_0 - C_t) \times 100}{C_0} \quad (2)$$

where q_t (mg/g) is the sorption capacity at time t; C_0 is the initial concentration of heavy metal ions (mg/L); C_t (mg/L) is the concentration of heavy metal ions at time t; V is the volume of reaction solutions, m is the mass of sorbent and removal efficiency (%) is the percentage of adsorbed heavy metal ions from solution.

3. Results and discussion

3.1. Magnetic property of bentonite-Fe_3O_4-MnO_2 with different MnO_2 loading

The magnetic property of bentonite-Fe_3O_4 and bentonite-Fe_3O_4-MnO_2 with different Fe/Mn ratio (2:1, 1:1, 1:1.5 and 1:2) was evaluated by examining the magnetic hysteresis loops at room temperature, as shown in Fig. 1a. All curves display a typical superparamagnetic property. The saturation magnetization (Ms) of bentonite-Fe_3O_4-MnO_2 with different Fe/Mn ratio (2:1, 1:1, 1:1.5 and 1:2) was 30.5, 23.5, 17.8 and 13.4 emu/g, respectively; all were lower than bentonite-Fe_3O_4 (38.1 emu/g). It can be observed that the saturation magnetization of magnetic adsorbents decreased as the amount of MnO_2 increased, since the non-magnetic MnO_2 induced a magnetic "dilution" of the sample. Nevertheless, the saturation magnetization of bentonite-Fe_3O_4-MnO_2 (1:2) is still enough to be separated with a magnet. The inset photograph shows that bentonite-Fe_3O_4-MnO_2 (1:2) could be easily separated in the presence of an external magnetic field.

In order to select the optimal loading ratios of MnO_2, Cd(II) adsorption capacity was tested. The effect of bentonite-Fe_3O_4 sorbents with different MnO_2 loading on Cd(II) uptake capacity is presented in Fig. 1b. It was demonstrated that the Cd(II) adsorption capacity increased with the increase of MnO_2 content, and almost reached the peak when the Fe:Mn was 1:1.5. Further increase of the Fe:Mn showed very little change on Cd(II) adsorption. Hence, considering both the saturation magnetization and Cd(II) adsorption, bentonite-Fe_3O_4-MnO_2 (1:1.5) was used for the further experiments.

3.2. Characterization of bentonite-Fe_3O_4-MnO_2

The XRD patterns of the adsorbents were shown in Fig. 2. For bentonite (Fig. 2a), two obvious diffraction peaks appear at 19.74° and 61.88°, which indicates the presence of montmorillonite, a main component of bentonite [31]. The peak at 26.56° is corresponding to SiO_2. Six well-dissolved diffraction peaks for the bentonite-Fe_3O_4, located at 30.10°, 35.44°, 43.06°, 53.68°, 57.04° and 62.58° in Fig. 2b, can be indexed as the (220), (311), (400), (442), (511) and (440) planes of Fe_3O_4 (JCPDS 65-3107) [17], indicating the successful integration of Fe_3O_4 particles on the surface of bentonite. For the bentonite-Fe_3O_4-MnO_2 (1:1.5) shown in Fig. 2, the characteristic peaks of Fe_3O_4 have weakened after the introduction of manganese oxides. Besides, no obvious diffraction peak of manganese oxides is detected which suggests that manganese oxides in the composite are likely to exist mainly in amorphous form. The surface area and active sites decrease significantly with increase in crystallinity [32]. The amorphous MnO_2 could contribute to the high surface area of bentonite-Fe_3O_4-MnO_2, to be presented next.

Based on the BET adsorption experiments, the pore parameters of bentonite, bentonite-Fe_3O_4 and bentonite-Fe_3O_4-MnO_2 (1:1.5) are shown in Table 1. The BET specific surface area of bentonite-Fe_3O_4-MnO_2 is 796.99 m^2/g, much higher than the values of bentonite (30.14 m^2/g) and bentonite-Fe_3O_4 (89.25 m^2/g). It is also much higher than that of a previously reported core-shell Fe_3O_4-MnO_2 nanomaterial (207.62 m^2/g) [33]. The pore volume of bentonite, bentonite-Fe_3O_4 and bentonite-Fe_3O_4-MnO_2 are 0.09, 0.28 and 1.70 cm^3/g, respectively. The bentonite-Fe_3O_4-MnO_2 composites show a significant increase of the BET surface area and pore volume compared with the

bentonite, which further confirm the successful pillaring of Fe_3O_4 and MnO_2 that increase the interlayer spacing. The average pore diameter of bentonite-Fe_3O_4-MnO_2 is 8.5 nm, which indicated that bentonite-Fe_3O_4-MnO_2 has a very porous structure.

The morphologies of the bentonite, bentonite-Fe_3O_4, bentonite-Fe_3O_4-MnO_2 (1:1.5) are illustrated in Fig.3. The SEM and TEM images of bentonite in Fig.3(a ,d) show a typical layer structures. SEM image of bentonite-Fe_3O_4 composite in Fig.3b shows that Fe_3O_4 nanoparticles are dispersed evenly on the surface or inserted between layers of the bentonite plates. The average size of Fe_3O_4 loaded on bentonite was found to be 13 nm (Fig. 3e). After immobilization of MnO_2 in the magnetic bentonite, the Fe_3O_4 nanoparticles and the MnO_2 sheets are assembled with the bentonite flakes randomly (Fig. 3(c, f)). EDX mapping of bentonite-Fe_3O_4-MnO_2 (1:1.5) nanocomposites confirmed the uniform distribution of Fe, Mn and O elements in the absorbent (EDX elemental mappings in Fig. S1).

Fig. 4 shows the loss of bentonite-Fe_3O_4-MnO_2 and the concentrations of dissolved Fe and Mn under HNO_3 solution with different pH. The bentonite-Fe_3O_4-MnO_2 (1:1.5) showed excellent stability at pH 5-10 while lost a little at pH 2-5, indicating a small part of adsorbent would dissolve in acid solution. When the solution pH $\geq$ 3, Fe and Mn concentrations were below 2 mg/L that met the national standard for waste water discharge. Therefore, bentonite-Fe_3O_4-MnO_2 is recommended to be used for solutions with pH $\geq$ 3.

3.3. Adsorption behavior

3.3.1. Adsorption kinetics of Cd(Ⅱ)

The effect of contact time on the sorption of Cd(II) by various adsorbents are shown in Fig. 5a. The adsorption of Cd(II) for bentonite-Fe_3O_4-MnO_2 was initially rapid within the first 5 min and then increased slowly and reached equilibrium within 30 min. Therefore, 2 h was chosen as the duration. According to previous studies, the fast Cd(Ⅱ) sorption at the beginning was attributed to the rapid diffusion of Cd(II) to the external surfaces of adsorbents and the slow process was ascribed to longer diffusion range of Cd(II) into the inner pores of adsorbents or the exchange with cations in the inner surface [34-37]. The results suggested that the adsorption process may consists of two stages, namely, electrostatic attraction and surface complexation or ion-exchange between the adsorbate and the adsorbent. Besides, the available adsorption sites were abundant for interacting with Cd(II) at first, then became less and less as the reaction progressed.

The pseudo-first-order kinetic model and pseudo-second-order kinetic model were employed to simulate the adsorption procedure and as shown as Eqs. (3) and (4), respectively.

$$q_t = q_e(1 - e^{-k_1 t}) \quad (3)$$

$$q_t = \frac{q_e^2 k_2 t}{1 + q_e k_2 t} \quad (4)$$

where q_t (mg/g) is the sorption capacity at time t; q_e (mg/g) is the sorption capacity at equilibrium; k_1 (min^{-1}) and k_2 ($g \cdot mg^{-1} \cdot min^{-1}$) is the equilibrium rate constants of the pseudo-first-order kinetic model and pseudo-second-order kinetic model, respectively.

Fig. 5a shows that the 3 samples displayed similar adsorption trend but with different

adsorption capacities. It is observed that the sorption capacity (q_e) of Cd(II) follows the order of bentonite-Fe_3O_4@MnO_2 (30.17 mg/g) > bentonite (27.43 mg/g) > bentonite-Fe_3O_4 (20.93 mg/g). The MnO_2 content on bentonite-Fe_3O_4-MnO_2 played an important role in the Cd(II) adsorption process. The presence of Fe_3O_4 occupied part of active sites on the bentonite surface, thus leading to the decrease of Cd(II) sorption, which is consistent with Chen and his coworkers' study [38].

The regression curves of the kinetic models are shown in Fig. 5(b-c). The corresponding kinetic parameters are presented in Table 2. As a result, the pseudo-second-order model was better to describe the adsorption process, as it has a higher correlation coefficient (R^2) of 0.99. This indicates that the adsorption of Cd(II) on bentonite-Fe_3O_4-MnO_2 was a chemisorption process [39].

3.3.2. Adsorption isotherms of Cd(II)

To evaluate the adsorption properties of the bentonite-Fe_3O_4-MnO_2 for Cd(II) removal from the aqueous solution, the adsorption isotherm experiments were conducted. The Lagmuir and Freundlich equations expressed in Eq.(5) and (6) were employed for isotherm fitting.

$$\frac{1}{q_e} = \frac{1}{K_L q_m} \cdot \frac{1}{C_e} + \frac{1}{q_m} \quad (5)$$

$$lnq_e = lnK_F + \frac{1}{n} lnC_e \quad (6)$$

where q_e (mg/g) is the amount of Cd(II) adsorbed per weight unit of adsorbent at

equilibrium, and C_e (mg/L) is the equilibrium concentration of Cd(Ⅱ). Here q_m (mg/g) is the maximum adsorption capacity and K_L is the Langmuir adsorption equilibrium constant. K_F is the Freundlich equilibrium constant indicative of adsorption capacity and n is the adsorption intensity. Generally, it is considered easy for adsorption when $1/n < 0.5$ whereas it is difficult adsorbed when $1/n>2$.

Fig. 6 displays the adsorption isotherms of Cd(II). All the isotherms showed a similar shape and were nonlinear over a wide range of aqueous equilibrium concentration. The fitted constants for the Langmuir and Freundlich isotherm models along with R^2 are listed in Table 3. It is evident that the Freundlich model (R^2=0.919) was better to describe the adsorption behavior of bentonite-Fe_3O_4-MnO_2 than the Langmiur equation did (R^2=0.882). The Langmiur model assumes that adsorption occurs on the homogeneous surface, while the Freundlich model describes the adsorption behavior on heterogeneous surface. Coupled with the porous and heterogeneous nature of bentonite-Fe_3O_4-MnO_2, we believe the Cd(II) adsorption on bentonite-Fe_3O_4-MnO_2 is better described by the Freundlich model.

To verify the advantage of the synthesized composites, a comparison between bentonite-Fe_3O_4-MnO_2 and some similar kind of reported adsorbents is provided in Table S1. The maximum Cd(II) adsorption capacity of bentonite-Fe_3O_4-MnO_2 was higher than bentonite-Fe_3O_4 due to the presence of MnO_2 and superior to the other similar adsorbents, but it was lower than that of Fe_3O_4-MnO_2 and Fe-Mn binary oxide.

The advantage of the current work includes the use of low cost bentonite clay minerals and the simplicity of the synthesis of bentonite-Fe_3O_4-MnO_2 composite. Furthermore, the magnetic property provides an easy way for particle separation.

3.3.3. Adsorption of trace Cd(II)

Taking the strict maximum contaminant level (MCL) standard of Cd(II) (= 5 μg/L) into consideration, it is important to examine the removal efficiency of bentonite-Fe_3O_4-MnO_2 for trace level of Cd(II). In this study, 100 μg/L was chosen as the initial Cd(II) concentration. Fig. 7 shows the residual Cd(II) concentrations and removal efficiency of Cd(II) by bentonite-Fe_3O_4-MnO_2. The observation indicates that the prepared adsorbent is effective for trace Cd(II) removal. At least 95.2% of Cd(II) were adsorbed when the adsorbent dosage was higher than 0.03 g/L, and the residual Cd(II) in the solution was less than 4.84 μg/L. This percentage meets the MCL standard for drinking water (≤ 5 μg/L according to the World Health Organization).

3.3.4. Effect of pH on the adsorption of Cd(II)

As the pH of solution is one of the most important factors affecting the adsorption process, the effect of pH on Cd(II) adsorption by bentonite-Fe_3O_4-MnO_2 was investigated at different pH values from 2.0 to 9.0. As shown in Fig. 8a, the amount of adsorbed Cd(II) increased with increasing pH. At lower pH, the competition between protons and Cd(II) for occupying the active sites would lead to the decrease of adsorption capacity. To further analyze the adsorption behavior, the zeta potential of

bentonite-Fe_3O_4-MnO_2 was determined by potentiometric analysis. From Fig. 8c, the charge of adsorbent surface was weakly positive at pH 3 and was increasingly negative as the pH increased. The pHzpc of bentonite-Fe_3O_4-MnO_2 was about 3.36. This means that when pH > 3.36, the electrostatic attraction strength between Cd(II) and adsorbent became stronger, which is consistent with the trend shown in Fig. 8a. Besides the electrostatic interaction, complexation and ion exchange might occur in an adsorption process for the adsorption of Cd(II) at pH 3 [40-41]. According to Zhong and his coworkers' study [37], Cd(II) started to precipitate from the solution in the form of $Cd(OH)_2$ when pH > 6.8. Therefore, pH 6 was selected as the enrichment acidity in the experiments.

3.3.5. Effect of ionic strength on the adsorption of Cd(II)

The effect of background ions is important in practical adsorption processes. A background ionic strength dependence study is also helpful to investigate the heavy metals adsorption mechanism. In this work, the effect of initial ionic strength on Cd(II) adsorption on bentonite-Fe_3O_4-MnO_2 was achieved by varying the concentrations of additive NaCl from 0.001 to 0.2 M. As shown in Fig. 8b, the uptake of Cd(II) from aqueous solution decreased from about 86.4% to 44.9% when the NaCl concentration changed from 0.001 to 0.2 M. A reasonable explanation is that there is a competitive adsorption between Cd(II) and Na^+ for the available active sites. At a lower ionic strength, there are more function groups available for Cd(II) uptake, thus the effect of Na^+ is insignificant. However, when the ionic strength is at a high level, the competition

between Cd(II) and Na^+ for the available sites becomes critical, resulting in low Cd(II) uptake. Similar trend has been reported by previous study too [42]. Accordingly, we believe cation exchange has contributed to the Cd(II) adsorption, because cation exchange is influenced by ionic strength whereas surface complexation is affected by pH values [43]. In the current work, Cd(II) adsorption on bentonite-Fe_3O_4-MnO_2 was mainly through outer-sphere adsorption, and the increase in solution ionic strength has decreased the adsorption of nonspecifically adsorbed ions on the adsorbent [44].

3.5. Cd(II) adsorption mechanism

3.5.1. FTIR analysis.

To better understand the adsorption mechanism of Cd(II) on bentonite-Fe_3O_4-MnO_2, the changes in FTIR spectrums recorded in the 4000–400 cm^{-1} range are shown in Fig. 9. In Fig. 9a, the peak near 3630 cm^{-1}, which corresponds to the stretching vibration of (Si, Al)-OH, obviously decreased after synthesis of Fe_3O_4 and MnO_2, probably due to the hydrogen bonding between the (Si, Al)-OH and hydroxyls on metal oxides. The bands around 1650 cm^{-1} and 3420 cm^{-1} were attributed to the bending vibration of coordinated water molecules of O-H and H-OH stretch vibrations [17]. The weakening of these two bands for bentonite-Fe_3O_4 might be caused by its production under heating and stirring, while the strengthening of these two bands for bentonite-Fe_3O_4-MnO_2 could be ascribed to more water on the surface and the O-H on MnO_2. The abundant O-H on bentonite-Fe_3O_4-MnO_2 is a good indication of it being a promising adsorbent. The apparent peak at 1040 cm^{-1} was assigned to the in-plane Si-O-Si stretching vibration

for bentonite [45], and was still stronger after the loading of metal oxides. This might be resulted from the overlap of Fe-OH and Mn-OH peaks [46]. The observed band at 800 cm^{-1} that is related to the stretching vibration of Si(Al)-O [47] decreased for two magnetic adsorbent samples. The peak at 916 cm^{-1} was resulted from O-H deformation vibration of inner Al-O-H groups [48]. Bentonite shows two peaks at 530 and 469 cm^{-1} representing the stretching vibration of Al-O-Si [49-50] and deformation vibration of Si-O-Si [48]. These peaks are much broader and stronger after adsorption because of the overlap with Fe-O peak from Fe_3O_4 [51]. In the spectrum of bentonite-Fe_3O_4-MnO_2, the expected characteristic absorption peaks of Mn-O at 450 cm^{-1}, 520 cm^{-1} and 720 cm^{-1} did not emerge for the amorphous MnO_2, which is consistent with XRD results [30].

Some obvious changes happened to the bentonite-Fe_3O_4-MnO_2 spectrum (Fig. 9b) after Cd(II) adsorption. The peaks near 3420 cm^{-1} and 1630 cm^{-1} attributed to –OH of the water molecules and metal oxides (Mn-OH) were much weaker, which can be explained by the interaction between hydroxyl groups on bentonite-Fe_3O_4-MnO_2 surface and Cd(II) in solution and possible formation of -O-Cd on the adsorbent [37, 52]. The peak at 3420 cm^{-1} shifted to 3255 cm^{-1} after the adsorption, which might be caused by the decrease of –OH and the presence of -O-Cd bond. After the adsorption, the peak at 1040 cm^{-1} corresponding to metal hydroxyl groups (Fe-OH, Mn-OH) also sharply decreased, which is attributed to the adsorption of Cd(II).

3.5.2. XPS analysis.

In order to further confirm the adsorption mechanism, the XPS spectra of the absorbent before and after Cd(Ⅱ) sorption were analyzed. The Fe 2p XPS in Fig. 10A shows the typical peaks located at 710.8eV and 723.8eV are assigned to Fe $2p_{2/3}$ and Fe $2p_{1/2}$ [53]. Fig. 11B depicts two bands with binding energies of 641.6 eV and 653.1 eV that assigned to Mn $2p_{2/3}$ and Mn $2p_{1/2}$ [53]. After Cd adsorption, the binding energy of Fe and Mn has not changed, indicating that bentonite-Fe_3O_4-MnO_2 composites are stable in Cd adsorption.

In Fig.11C, the O 1s XPS spectra was divided into three peaks corresponding to the oxygen in the lattice (in the form of O_2 from metal oxide) at 529.2 eV, in the surface hydroxyl group (–OH, hydroxyl bonded to metal such as Fe–OH and Mn–OH) at 531.5 eV and in the outer-most layer of H_2O adsorbed at 533.1 eV based on the binding energy of different oxygen species [54]. After Cd adsorption, the area ratios of the peaks at 533.1 eV changed slightly suggesting that the adsorbed H_2O are not involved in Cd sorption. Meanwhile the surface hydroxyl groups located at 531.5 eV decreased from 37.1% to 24.3%, indicating that surface hydroxyl groups are involved in the adsorption of Cd. The increased proportion of oxygen in the lattice at 529.0 eV from 54.4% to 65.3% could be originated from the formation of M-O on the surface and Cd-O groups in the adsorbed Cd species. It can be concluded that the surface hydroxyl groups (M-OH) groups on the absorbent surface are responsible for Cd(II) adsorption with O atoms acting as binding sites for Cd.

Based on the above analyses, we propose the possible mechanism of Cd(II) adsorption on bentonite-Fe_3O_4-MnO_2 composites as shown in Scheme 1. The adsorption processes

can be generally divided into electrostatic interaction and chemical binding mechanisms. In the adsorption process, bentonite-Fe_3O_4-MnO_2 is negatively charged when pH is above 3.36, and the high surface negative charges of absorbent facilitated the fast migration of the positively charged Cd(II) to the periphery of bentonite-Fe_3O_4-MnO_2 through the electrostatic attractions. Furthermore, the adsorbed Cd(II) formed complexation with the surface hydroxyl groups.

3.6. Regeneration of bentonite-Fe_3O_4-MnO_2.

In view of the practical of the adsorbent, the recycling and reuse is an important consideration. Based on the early results from Fig. 4, HNO_3 solution with pH = 3 would be an ideal condition for Cd(II) desorption due to the acceptable Fe and Mn dissolution and poor adsorption capacity at that pH. The adsorption−desorption cycles were repeated five times using the same batch of bentonite-Fe_3O_4-MnO_2 (Fig. 11a). Compared to the fresh adsorbent, the adsorption capacity at the second cycle decreased to 83.7% of the first cycle, and further to 77.0% in the third cycle. After which, it remained almost unchanged in the subsequent cycles. The decrease in the adsorption capacity may be partly attributed to the incomplete desorption of Cd(II) from the surface of bentonite-Fe_3O_4-MnO_2 [37,55]. Also when Cd(II) ions go into the vacant site of MnO_2, desorption may be more difficult [55]. After five cycles, the adsorption capacity, the magnetic intensity of bentonite-Fe_3O_4-MnO_2 did not decrease and the adsorbent could be separated from solution quickly. Fig. 11(b, c) shows the representative SEM and TEM images of regenerated composites after the fifth cycle.

The regenerated adsorbent still retained nanoparticle structure and shows little difference with the fresh adsorbent. Furthermore, EDX elements analysis shown that little Cd(II) remained on the surface of the bentonite-Fe_3O_4-MnO_2 after the fifth cycle (Fig.11c). Therefore, the prepared bentonite-Fe_3O_4-MnO_2 can be easily recycled and reused, which supports their long-term use in water purification.

4. CONCLUSION

The synthesized bentonite-Fe_3O_4-MnO_2 combined the high surface area of bentonite and manganese dioxide, and the magnetic property of Fe_3O_4, hence the adsorbent showed a good recovery and reusability in removing Cd(II) from solution. The maximal adsorption capacities for Cd(II) was 35.35mg/g. The adsorption capacity was found to increase with increasing pH. The adsorption was also dependent on the ionic strength, which implied that Cd(II) has participated in the formation of outer-sphere complexes on bentonite-Fe_3O_4-MnO_2 surface. According to the FTIR and XPS analyses, the surface hydroxyl groups of bentonite-Fe_3O_4-MnO_2 have played a critical role in the Cd(II) adsorption process, and there is a possibility of -O-Cd bonding formation during the adsorption. Moreover, the prepared bentonite-Fe_3O_4-MnO_2 can be easily recycled and reused. Considering the simple fabrication procedure, environmental friendliness, excellent removal capacity, and good regeneration performance of bentonite-Fe_3O_4-MnO_2, it is expected that bentonite-Fe_3O_4-MnO_2 has broad applications for the treatment of heavy metal ions from aqueous systems.

ACKNOWLEDGMENTS

This work was supported by the National Natural Science Foundation of China (No. 21107097), the Zhejiang Province Natural Science Foundation of China (No. Y5110118).

REFERENCES

[1] J.O. Nriagu, J.M. Pacyna, Quantitative assessment of worldwide contamination of air, water and soils by trace metals. Nature 333(198) 134-139.

[2] H.P. Zhang, L.Q. Gu, L. Zhang, S.R. Zheng, H.Q. Wan, J.Y. Sun, D.Q. Zhu, Z.Y. Xu, Removal of aqueous Pb(Ⅱ) by adsorption on Al_2O_3-pillared layered MnO_2, Appl. Surf. Sci. 406 (2017) 330-338.

[3] M.P. Waalkes, Cadmium carcinogenesis in review, J. Inorg. Biochem. 79 (2000) 241-244.

[4] H.Y. Jiang, Q.X. Zhao, Y. Zeng, Removal of Cd(Ⅱ) and Pb(Ⅱ) from aqueous solutions by modified polyvinyl alcohol, Desalin. Water Treat. 57 (2016) 6452-6462.

[5] G. Chen, K.J. Shah, L. Shi, P.C. Chiang, Removal of Cd(Ⅱ) and Pb(Ⅱ) ions from aqueous solutions by synthetic mineral adsorbent: Performance and mechanisms, Appl. Surf. Sci. 409 (2017) 296-305.

[6] A.K. Thakur, G.M. Nisola, L.A. Limjuco, K.J. Parohinog, R.E.C. Torrejos, V.K. Shahi, W.J. Chung, Polyethylenimine-modified mesoporous silica adsorbent for simultaneous removal of Cd(Ⅱ) and Ni(Ⅱ) from aqueous solution, J. Ind. Eng. Chem. 49 (2017) 133-144.

[7] A.A. Taha, M.A. Shreadah, A.M. Ahmed, H.F. Heiba, Multi-component adsorption of Pb(Ⅱ), Cd(Ⅱ), and Ni(Ⅱ) onto Egyptian Na-activated bentonite; equilibrium, kinetics, thermodynamics, and application for seawater desalination, J. Environ. Chem. Eng. 4 (2016) 1166-1180.

[8] G.X. Zhao, H.X. Zhang, Q.H. Fan, X.M. Ren, J.X. Li, Y.X. Chen, X.K. Wang, Sorption of copper(Ⅱ)

onto super-adsorbent of bentonite-polyacrylamide composites, J. Hazard. Mater. 173 (2010) 661-668.

[9] A.S. Ozcan, O. Gok, A. Ozcan, Adsorption of lead(Ⅱ) ions onto 8-hydroxy quinoline-immobilized bentonite, J. Hazard. Mater. 161 (2009) 499-509.

[10] A. Kaya, A.H. Oren, Adsorption of zinc from aqueous solutions to bentonite, J. Hazard. Mater. 125 (2005) 183-189.

[11] L.N. Shi, X. Zhang, Z.L. Chen, Removal of Chromium (VI) from wastewater using bentonite-supported nanoscale zero-valent iron, Water Res. 45 (2011) 886-892.

[12] M.T. Azar, M. Leili, F. Taherkhani, A. Bhatnagar, A comparative study for the removal of aniline from aqueous solutions using modified bentonite and activated carbon, Desalin. Water Treat. 57 (2016) 24430-24443.

[13] S.Q. Kong, Y.X. Wang, Q.H. Hu, A.K. Olusegun, Magnetic nanoscale Fe-Mn binary oxides loaded zeolite for arsenic removal from synthetic groundwater, Colloid. Surface. A 457 (2014) 220-227.

[14] H.J. Cui, J.K. Cai, H. Zhao, B.L. Yuan, C.L. Ai, M.L. Fu, Fabrication of magnetic porous Fe-Mn binary oxide nanowires with superior capability for removal of As(III) from water, J. Hazard. Mater. 279 (2014) 26-31.

[15] A. Mehdinia, M. Jebeliyan, T.B. Kayyal, A. Jabbari, Rattle-type Fe_3O_4@SnO_2 core-shell nanoparticles for dispersive solid-phase extraction of mercury ions, Microchim. Acta. 184 (2017) 707-713.

[16] H. Luo, S.X. Zhang, X.Y. Li, X. Liu, Q. Xu, J.S. Liu, Z.H. Wang, Tannic acid modified Fe_3O_4 core-shell nanoparticles for adsorption of Pb^{2+} and Hg^{2+}, J. Taiwan Inst. Chem. E., 72 (2017) 163-170.

[17] L.G. Yan, S. Li, H.Q. Yu, R.R. Shan, B. Du, T.T. Liu, Facile solvothermal synthesis of Fe_3O_4/bentonite for efficient removal of heavy metals from aqueous solution, Powder Technol.301 (2016)

632-640.

[18] J. Gimenez, M. Martinez, J. de Pablo, M. Rovira, L. Duro, Arsenic sorption onto natural hematite, magnetite, and goethite, J. Hazard. Mater. 141 (2007) 575-580.

[19] J.E. Post. Manganese oxide minerals: Crystal structures and econmic and environmental significance. Proc. Natl. Acad. Sci. U.S.A. 96(1999):3447-3454

[20] L.J. Dong, Z.L. Zhu, H.M. Ma, Y.L. Qiu, J.F. Zhao, Simultaneous adsorption of lead and cadmium on MnO_2-loaded resin, J. Environ. Sci. 22 (2010) 225-229.

[21] Q.D. Qin, Q.Q. Wang, D.F. Fu, J. Ma. An efficient approach for Pb(Ⅱ) and Cd(Ⅱ) removal using manganese dioxide formed in situ. Chem. Eng. J. 172(2011):68-74.

[22] Q. Su, B.C. Pan, S.L. Wan, W.M. Zhang, L. Lv. Use of hydrous manganese dioxide as potential sorbent for selective removal of lead, cadmium, and zinc ions from water. J. Colloid Interf. Sci. 349(2010):607-612.

[23] Z.M. Wang, S.W. Lee, J.G. Catalano, J.S. Lezama-Pacheco, J.R. Bargar, B.M. Tebo, D.E. Giammar, Adsorption of Uranium(VI) to Manganese Oxides: X-ray Absorption Spectroscopy and Surface Complexation Modeling, Environ. Sci. Technol. 47 (2013) 850-858.

[24] C. Shan, M.P. Tong, Efficient removal of trace arsenite through oxidation and adsorption by magnetic nanoparticles modified with Fe-Mn binary oxide, Water Res. 47 (2013) 3411-3421.

[25] E.J. Kim, C.S. Lee, Y.Y. Chang, Y.S. Chang. Hierarchically structured manganese oxide-coated magnetic nanocomposites for the efficient removal of heavy metal ions from aqueous systems. ACS appl. Mater. Inter. 5(2013):9628-9634.

[26] J. Chen, F. He, H. Zhang, X. Zhang, G. Zhang, G. Yuan, Novel Core–Shell Structured Mn–Fe/MnO_2 Magnetic Nanoparticles for Enhanced Pb(Ⅱ) Removal from Aqueous Solution, Ind. Eng. Chem. Res. 53

(2014) 18481-18488.

[27] X.B. Luo, C.C. Wang, S.L. Luo, R.Z. Dong, X.M. Tu, G.S. Zeng. Adsorption of As (III) and As(V) from water using magnetite Fe3O4-reduced graphite oxide-MnO2 nanocomposites. Chem. Eng. J. 187(2012) 45-52.

[28] L.Y. Jiang, L. Liu, S.D. Xiao, J.M. Chen, Preparation of a novel manganese oxide-modified diatomite and its aniline removal mechanism from solution, Chem. Eng. J. 284 (2016) 609-619.

[29] W.L. Guo, W. Hu, J.M. Pan, H.C. Zhou, W. Guan, X. Wang, J.D. Dai, L.C. Xu, Selective adsorption and separation of BPA from aqueous solution using novel molecularly imprinted polymers based on kaolinite/Fe_3O_4 composites, Chem. Eng. J. 171 (2011) 603-611.

[30] J. Zhu, S.A. Baig, T.T. Sheng, Z.M. Lou, Z.X. Wang, X.H. Xu, Fe_3O_4 and MnO_2 assembled on honeycomb briquette cinders (HBC) for arsenic removal from aqueous solutions, J. Hazard. Mater. 286 (2015) 220-228.

[31] Y.G. Chen, B.Z. Zhu, D. B. Wu, Q.G. Wang, Y.H. Yang, W.M. Ye, Eu(III) adsorption using di(2-thylhexly) phosphoric acid-immobilized magnetic GMZ bentonite. Chem. Eng. J. 181-182(2012) 387-396.

[32] L.Y. Jiang, S.D. Xiao, J.M. Chen, Removal behavior and mechanism of Co(Ⅱ) on the surface of Fe-Mn binary oxide adsorbent, Colloid. Surface. A, 479 (2015) 1-10.

[33] J. Liu, Z.W. Zhao, P.H. Shao, F.Y. Cui, Activation of peroxymonosulfate with magnetic Fe_3O_4-MnO_2 core-shell nanocomposites for 4-chlorophenol degradation, Chem. Eng. J. 262 (2015) 854-861.

[34] G.D. Sheng, J.X. Li, D.D. Shao, J. Hu, C.L. Chen, Y.X. Chen, X.K. Wang, Adsorption of copper(Ⅱ) on multiwalled carbon nanotubes in the absence and presence of humic or fulvic acids, J. Hazard. Mater. 178 (2010) 333-340.

[35] G.D. Sheng, D.D. Shao, X.M. Ren, X.Q. Wang, J.X. Li, Y.X. Chen, X.K. Wang, Kinetics and thermodynamics of adsorption of ionizable aromatic compounds from aqueous solutions by as-prepared and oxidized multiwalled carbon nanotubes, J. Hazard. Mater. 178 (2010) 505-516.

[36] C.L. Chen, J. Hu, D. Xu, X.L. Tan, Y.D. Meng, X.K. Wang, Surface complexation modeling of Sr(Ⅱ) and Eu(III) adsorption onto oxidized multiwall carbon nanotubes, J. Colloid. Interf .Sci. 323 (2008) 33-41.

[37] L.B. Zhong, J. Yin, S.G. Liu, Q. Liu, Y.S. Yang, Y.M. Zheng, Facile one-pot synthesis of urchin-like Fe-Mn binary oxide nanoparticles for effective adsorption of Cd(Ⅱ) from water, Rsc Adv., 6 (2016) 103438-103445.

[38] L. Chen, Y. Huang, L.L. Huang, B. Liu, G. Wang, S.M. Yu, Characterization of Co(Ⅱ) removal from aqueous solution using bentonite/iron oxide magnetic composites, J. Radioanal. Nucl. Ch., 290 (2011) 675-684.

[39] G.S. Zhang, Z.M. Ren, X.W. Zhang, J. Chen, Nanostructured iron(III)-copper(Ⅱ) binary oxide: A novel adsorbent for enhanced arsenic removal from aqueous solutions, Water Res. 47 (2013) 4022-4031.

[40] V.K. Gupta, A. Nayak, Cadmium removal and recovery from aqueous solutions by novel adsorbents prepared from orange peel and Fe_2O_3 nanoparticles, Chem. Eng. J. 180 (2012) 81-90.

[41] S.M. Lee, C. Laldawngliana, D. Tiwari, Iron oxide nano-particles-immobilized-sand material in the treatment of Cu(Ⅱ), Cd(Ⅱ) and Pb(Ⅱ) contaminated waste waters, Chem. Eng. J. 195 (2012) 103-111.

[42] L. Peng, Q.R. Zeng, B.Q. Tie, M. Lei, J. Yang, S. Luo, Z.G. Song, Manganese Dioxide nanosheet suspension: A novel absorbent for Cadmium(Ⅱ) contamination in waterbody, J. Colloid. Interf. Sci. 456 (2015) 108-115.

[43] Y.G. Chen, W.M. Ye, X.M. Yang, F.Y. Deng, Y. He, Effect of contact time, pH, and ionic strength

on Cd(Ⅱ) adsorption from aqueous solution onto bentonite from Gaomiaozi, China, Environ. Earth. Sci. 64 (2011) 329-336.

[44] Y.M. Zheng, L. Yu, J.P. Chen, Removal of methylated arsenic using a nanostructured zirconia-based sorbent: Process performance and adsorption chemistry, J. Colloid. Interf. Sci. 367 (2012) 362-369.

[45] H.L. Zhang, T.F. Ren, Y.J. Ji, L.G. Han, Y.G. Wu, H.Z. Song, L.B. Bai, X.W. Ba, Selective Modification of Halloysite Nanotubes with 1-Pyrenylboronic Acid: A Novel Fluorescence Probe with Highly Selective and Sensitive Response to Hyperoxide, Acs Appl. Mater. Inter. 7 (2015) 23805-23811.

[46] R.P. Liu, F. Liu, C.Z. Hu, Z. He, H.J. Liu, J.H. Qu, Simultaneous removal of Cd(Ⅱ) and Sb(V) by Fe-Mn binary oxide: Positive effects of Cd(Ⅱ) on Sb(V) adsorption, J. Hazard. Mater. 300 (2015) 847-854.

[47] Y. Fan, F.S. Zhang, Y.N. Feng, An effective adsorbent developed from municipal solid waste and coal co-combustion ash for As(V) removal from aqueous solution, J. Hazard. Mater. 159 (2008) 313-318.

[48] M. Fayazi, M.A. Taher, D. Afzali, A. Mostafavi, Fe_3O_4 and MnO_2 assembled on halloysite nanotubes: A highly efficient solid-phase extractant for electrochemical detection of mercury(Ⅱ) ions, Sensor. Actuat. B-Chem. 228 (2016) 1-9.

[49] J.D. Dai, X. Wei, Z.J. Cao, Z.P. Zhou, P. Yu, J.M. Pan, T.B. Zou, C.X. Li, Y.S. Yan, Highly-controllable imprinted polymer nanoshell at the surface of magnetic halloysite nanotubes for selective recognition and rapid adsorption of tetracycline, Rsc Adv. 4 (2014) 7967-7978.

[50] S. Hashemian, H. Saffari, S. Ragabion, Adsorption of Cobalt(Ⅱ) from Aqueous Solutions by Fe_3O_4/Bentonite Nanocomposite, Water Air Soil Poll. 226 (2015).

[51] J.H. Meng, G.Q. Yang, L.M. Yan, X.Y. Wang, Synthesis and characterization of magnetic nanometer pigment Fe_3O_4, Dyes Pigments 66 (2005) 109-113.

[52] Y.X. Xia, L.Y. Meng, Y.J. Jiang, Y.S. Zhang, X.X. Dai, M.J. Zhao, Facile preparation of MnO_2 functionalized baker's yeast composites and their adsorption mechanism for Cadmium, Chem. Eng. J. 259 (2015) 927-935.

[53] J. Mei, L. Zhang, Y. Niu. Fabrication of the magnetic manganese dioxide/graphene nanocomposite and its application in dye removal from the aqueous solution at room temperature. Mater. Res. Bull. 70(2015) 82-86.

[54] B. Peng, T.T. Song, T. Wang, L.Y. Chai, W.C. Yang, X.R. Li, C.F. Li, H.Y. Wang, Facile synthesis of Fe_3O_4 synthesis of Fe_3O_4@$Cu(OH)_2$ composites and their arsenic adsorption application. Chem. Eng. J. 299(2016) 15-22.

[55] E.J. Kim, C.S. Lee, Y.Y. Chang, Y.S. Chang, Hierarchically Structured Manganese Oxide-Coated Magnetic Nanocomposites for the Efficient Removal of Heavy Metal Ions from Aqueous Systems, Acs Appl. Mater. Inter. 5 (2013) 9628-9634.

SUPPORTING INFORMATION

Fabrication of magnetic bentonite layered MnO_2 and its application in Cd(Ⅱ) adsorption from aqueous solution

Liying Jiang[1]*, Qichao Ye[1], Jianmeng Chen[1], Zhong Chen*[2], Youli Gu[1], Xiang Cao[1]

1. College of Environment, Zhejiang University of Technology, Hangzhou 310032, China
2. School of Materials Science and Engineering, Nanyang Technological University, 50 Nanyang Avenue, Singapore 639798, Singapore

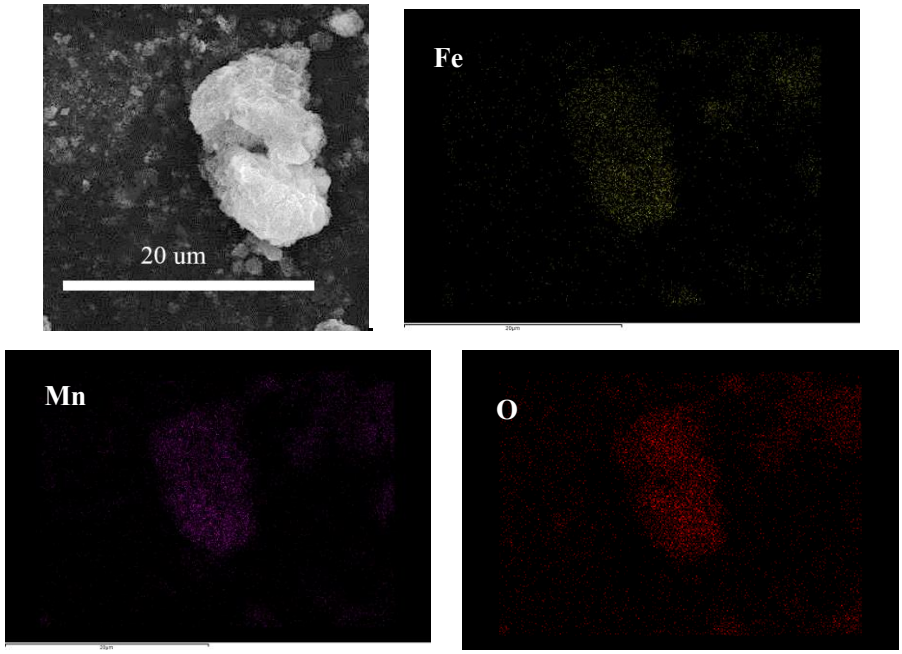

Fig. 1S. Typical elemental mappings of as-synthesized bentonite-Fe_3O_4-MnO_2

Table S1. Comparison of the maximum adsorption capacities of Cd(Ⅱ) onto various clay mineral-based adsorbents

Adsorbent sample	Qm (mg/g)	References
Bentonite-Fe_3O_4-MnO_2	35.35	This work
Bentonite-Fe_3O_4	21.7	[1]
Fe_3O_4-MnO_2	53.2	[2]
Fe-Mn binary oxide	74.76	[3]
Fe-montmorillonite	25.7	[4]
Fe_3O_4/Mg-Al-CO_3-LDH	45.6	[5]
Z0.4-AlPMt	13.04	[6]

References:

[1] L.G. Yan, L. Shuang, H.Q. Yu, R.R. Shan. D. Bin, T.T. Liu. Facile solvothermal synthesis of Fe_3O_4/bentonite for efficient removal of heavy metals from aqueous solution. Powder Technol., 301(2016) 632-640.

[2] E. J. Kim, C.S. Lee, Y.Y. Chang, Y.S. Chang. Hierarchically structured manganese oxide-coated magnetic nanocomposites for the efficient removal of heavy metal ions from aqueous system. ACS appl. Mater. Interfaces, 5(2013) 9628-9634.

[3] R.R. Shan, L.G. Yan, K. Yang, Y. F. Hao, B. Du. Adsorption of Cd(Ⅱ) by Mg-Al-CO_3- and magnetic Fe_3O_4/Mg-Al-CO_3-layered double hydroxides: kinetic, isothermal, thermodynamic and mechanistic studies. J. Hazard. Mater. 299(2015) 42-49

[4] P.X. Wu, W.M. Wu, S.Z. Li, N. Xing, N.W. Zhu, P. Li, J.H. Wu, C. Yang, Z. Dang, Removal of Cd^{2+} from aqueous solution by adsorption using Fe-montmorillonite. J. Hazard. Mater. 169(2009) 824-830

[5] L.Y. Ma, J.X. Zhu, Y.F. Xi, R.L. Zhu, H.P. He, X.L. Liang, G.A. Ayoko. Adsorption of phenol, phosphate and Cd(Ⅱ) by inorganic-organic montmorillonites: A comparative study of single and multiple solute. Colloid. Surface. A, 497(2016) 63-71

[6] L.B. Zhong, J. Yin, S.G. Liu, Q. Liu, Y.S. Yang, Y.M. Zheng, Facile one-pot synthesis of urchin-like

Fe-Mn binary oxide nanoparticles for effective adsorption of Cd(Ⅱ) from water. Rsc adv. 6(2016) 103438-103445.

Table S2. The binding energy values of the Fe 2p, Mn 2p, C 1s, O 1s of bentonite-Fe_3O_4-MnO_2 before and after Cd(II) sorption

Sample	Bentonite-Fe_3O_4-MnO_2		Ben--Fe_3O_4-MnO_2 +Cd		
	Binding energy (eV)	Area (%)	Binding energy (eV)	Area (%)	Bonds
Fe 2p	722.9	41.4	723.4	44.7	Fe $2p_{1/2}$
	710.7	58.6	710.3	55.3	Fe $2p_{2/3}$
Mn 2p	653.1	37.8	652.8	34.5	Mn $2p_{1/2}$
	641.6	62.2	641.4	65.5	Mn $2p_{2/3}$
O 1s	528.8	54.4	529.2	65.3	M-O
	531.1	37.1	531.3	24.3	M-OH
	533.0	8.5	533.1	10.4	H-O-H
C 1s	284.5	68.3	284.0	61.2	C-C, C-H
	286.5	9.0	286.6	15.1	C-O
	288.2	22.7	288.2	23.7	C=O

Figure Caption

Fig. 1. Magnetization curves (a) and adsorption capacity (b) of bentonite-Fe_3O_4-MnO_2 with different MnO_2 loading (top inset, photographs showing the states of bentonite-Fe_3O_4-MnO_2 (1:2) before and after placing a magnet).

Fig. 2. XRD patterns of bentonite (a), bentonite-Fe_3O_4 (b) and bentonite-Fe_3O_4-MnO_2 (1:1.5) (c)

Fig. 3. SEM and TEM images of bentonite (a, d); bentonite-Fe_3O_4 (b,e); bentonite-Fe_3O_4-MnO_2 (c, f); and EDX spectrum of bentonite-Fe_3O_4-MnO_2 (g)

Fig. 4. The stability of bentonite-Fe_3O_4-MnO_2 and residual Fe and Mn concentration in solution with varying pH

Fig. 5. (a) Effects of reaction time on Cd(II) adsorption by absorbents; (b) the pseudo-first-order and (c) the pseudo-second-order kinetic models for Cd(II) on the bentonite-Fe_3O_4-MnO_2

Fig. 6. Adsorption isotherm for Cd(II) adsorption onto bentonite-Fe_3O_4-MnO_2

Fig. 7 Removal of trace level of Cd(II) using bentonite-Fe_3O_4-MnO_2 with different dosages

Fig. 8. Effects of pH (a) and ionic strength (b) on the adsorption of Cd(II) by bentonite-Fe_3O_4-MnO_2; and determination of pH_{PZC} of three adsorbents (c)

Fig. 9. The FTIR spectra of bentonite, bentonite-Fe_3O_4 and bentonite-Fe_3O_4-MnO_2 (a); The FTIR spectra of bentonite-Fe_3O_4-MnO_2 before and after reaction with Cd(II) (b)

Fig. 10. Fe 2p(A), Mn 2p(B), O 1s (C) and C 1s (D) XPS spectra of bentonite-Fe_3O_4-MnO_2 (a), bentonite-Fe_3O_4-MnO_2 with Cd(II) adsorbed (b)

Fig. 11. Cd(II) removal by bentonite-Fe_3O_4-MnO_2 over five successive adsorption-desorption cycles (a); SEM image (b), TEM image (c) and EDX spectrum (d) of regenerated bentonite-Fe_3O_4-MnO_2

Scheme 1. Cd(II) adsorption mechanism onto bentonite-Fe_3O_4-MnO_2

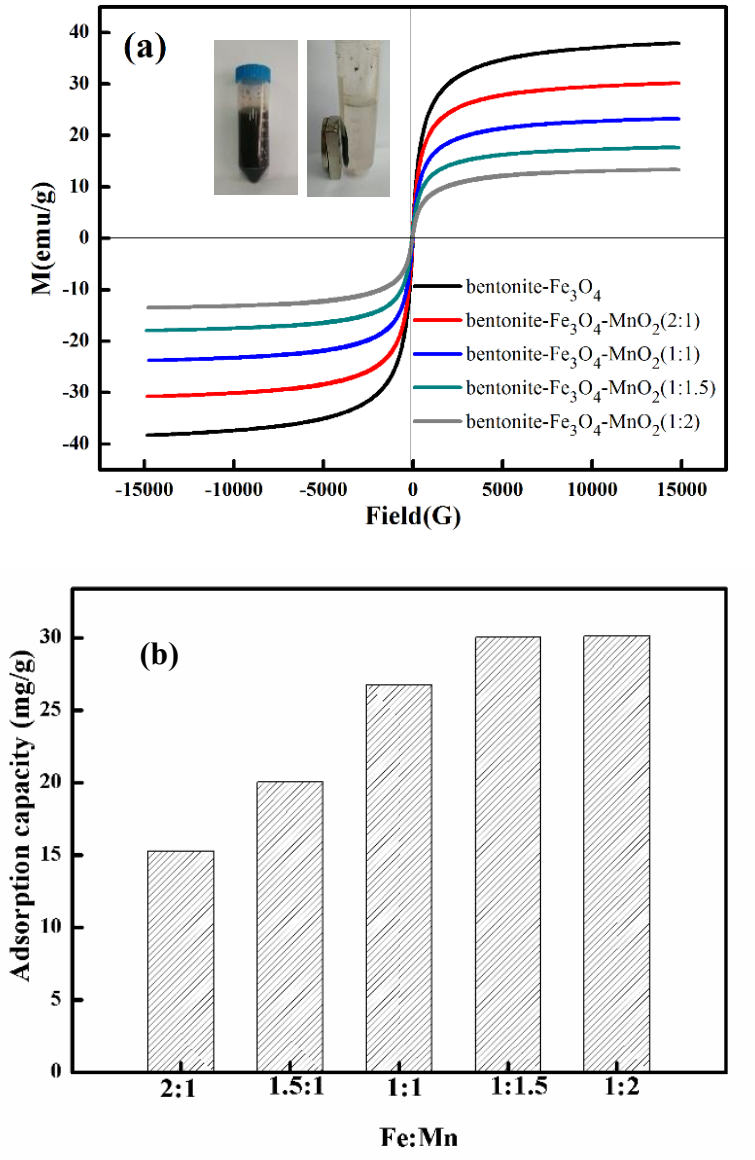

Fig. 1. Magnetization curves (a) and adsorption capacity (b) of bentonite-Fe_3O_4-MnO_2 with different MnO_2 loading (top inset, photographs showing the states of bentonite-Fe_3O_4-MnO_2 (1:2) before and after placing a magnet)

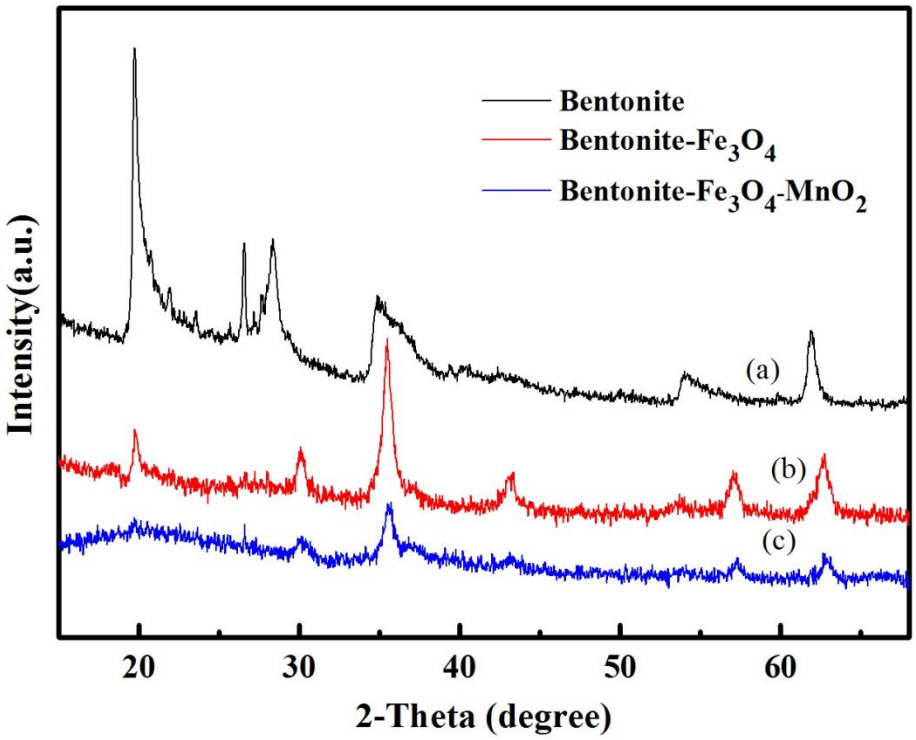

Fig. 2. XRD patterns of bentonite (a), bentonite -Fe_3O_4 (b) and bentonite-Fe_3O_4-MnO_2 (1:1.5) (c)

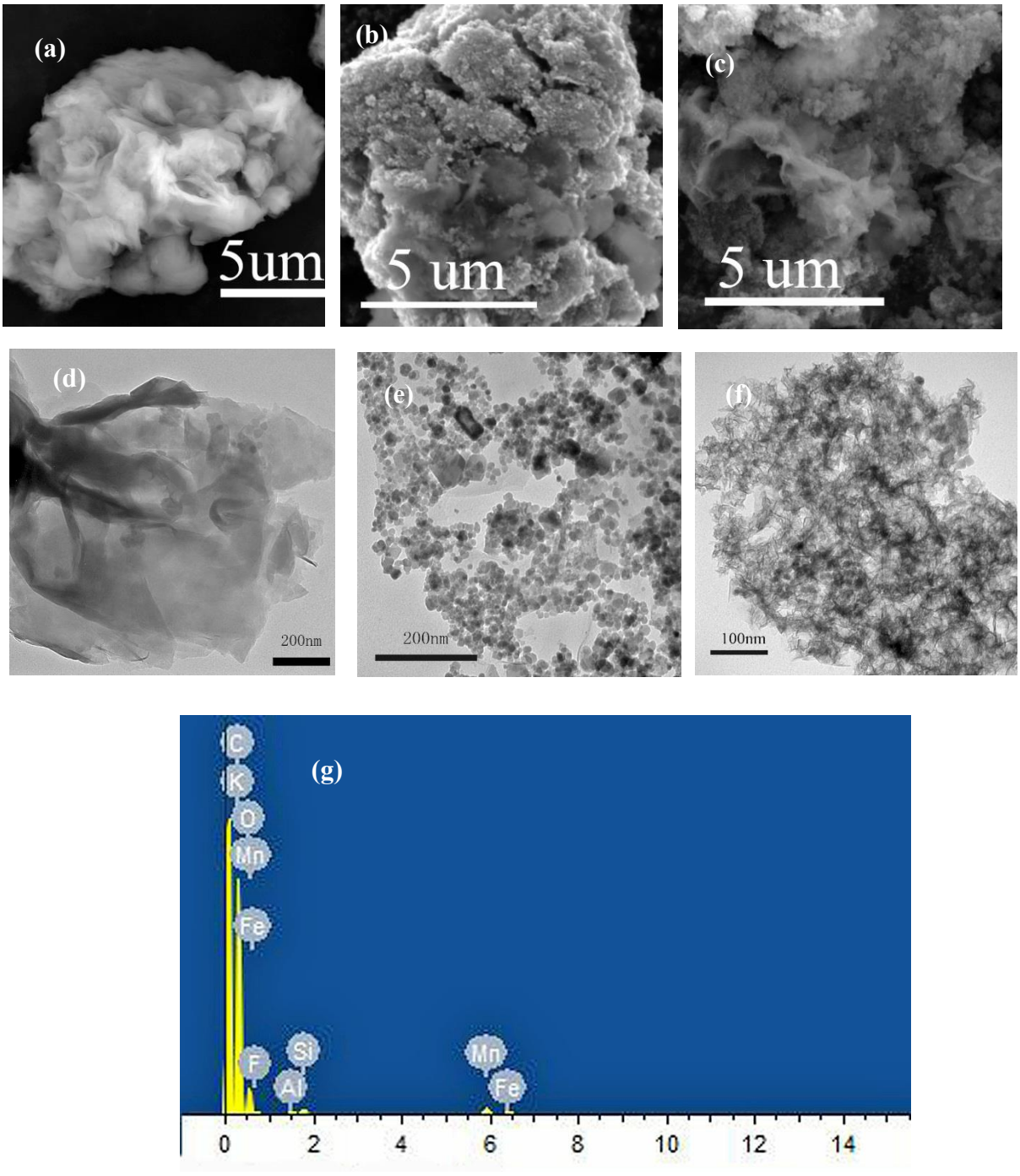

Fig. 3. SEM and TEM images of bentonite (a, d); bentonite-Fe_3O_4 (b,e); bentonite-Fe_3O_4-MnO_2 (c, f); and EDX spectrum of bentonite-Fe_3O_4-MnO_2 (g)

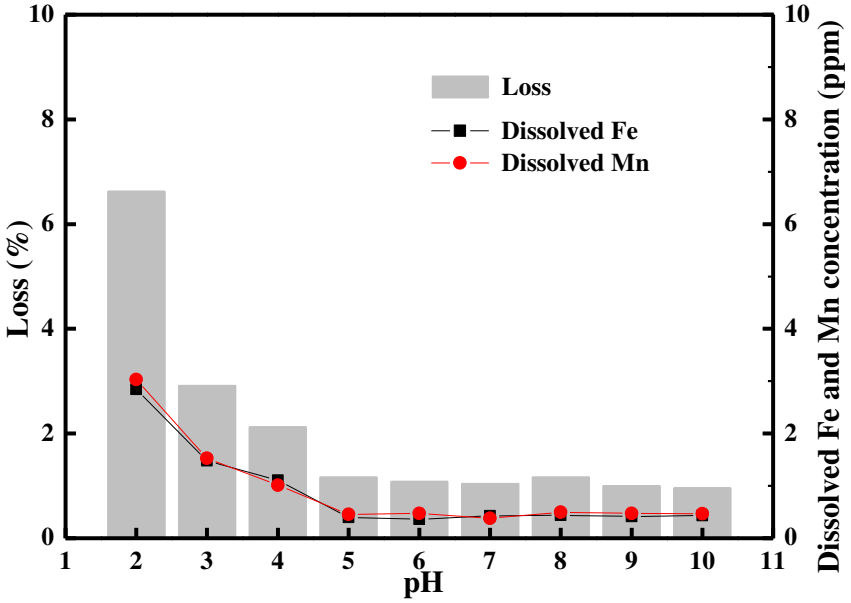

Fig. 4. The stability of bentonite-Fe_3O_4-MnO_2 and residual Fe and Mn concentration in solution with varying pH.

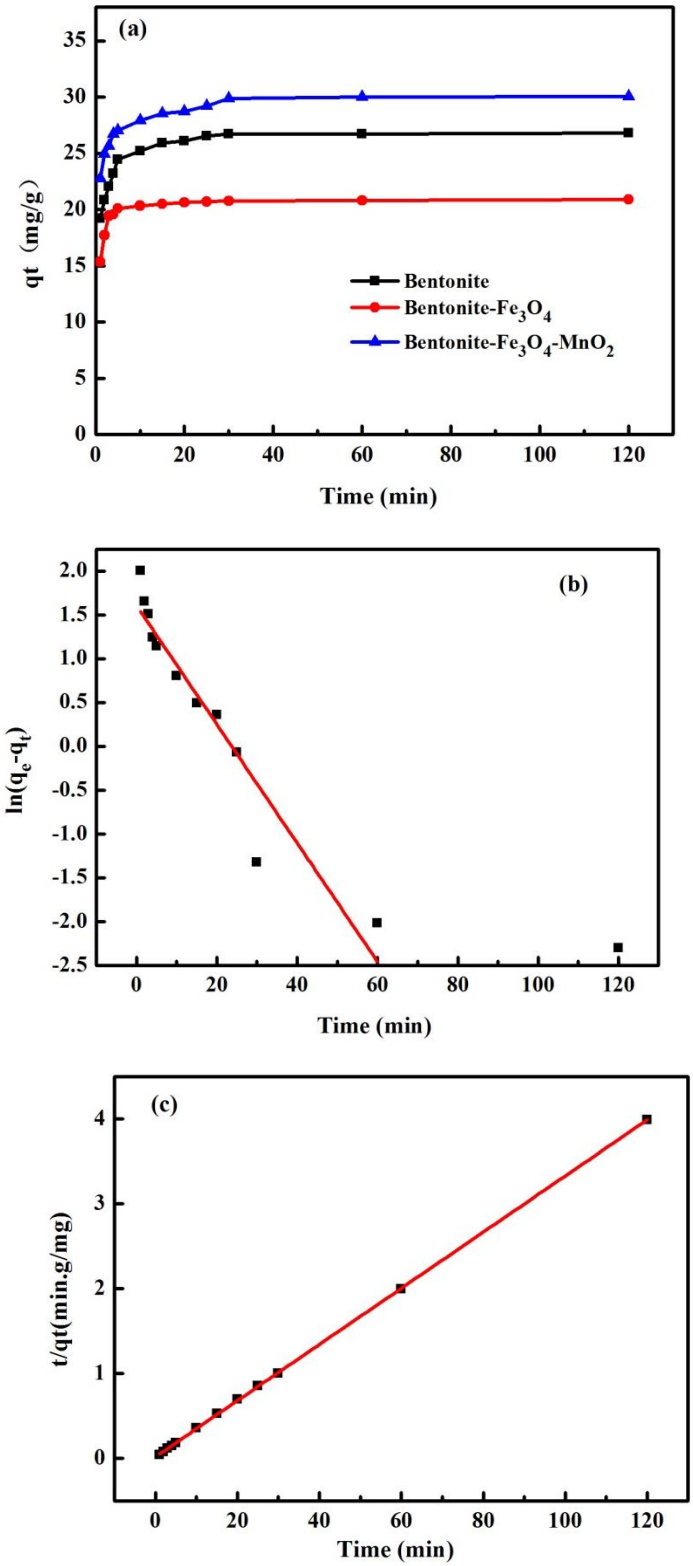

Fig. 5. (a) Effects of reaction time on Cd(II) adsorption by absorbents; (b) the pseudo-first-order and (c) the pseudo-second-order kinetic models for Cd(II) on the bentonite-Fe_3O_4-MnO_2

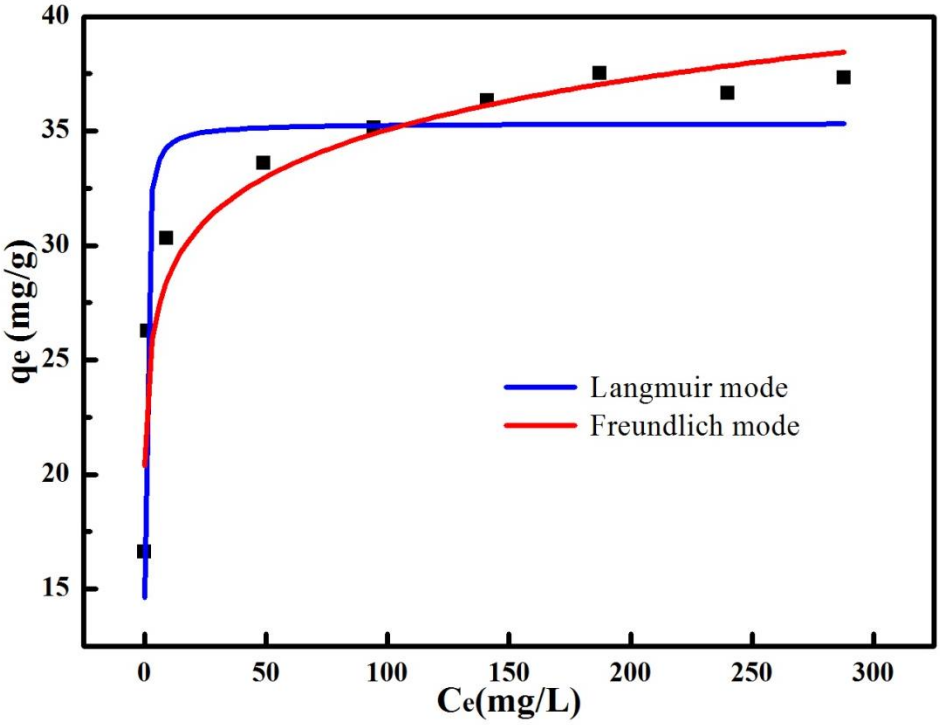

Fig. 6. Adsorption isotherm for Cd(II) adsorption onto bentonite-Fe_3O_4-MnO_2

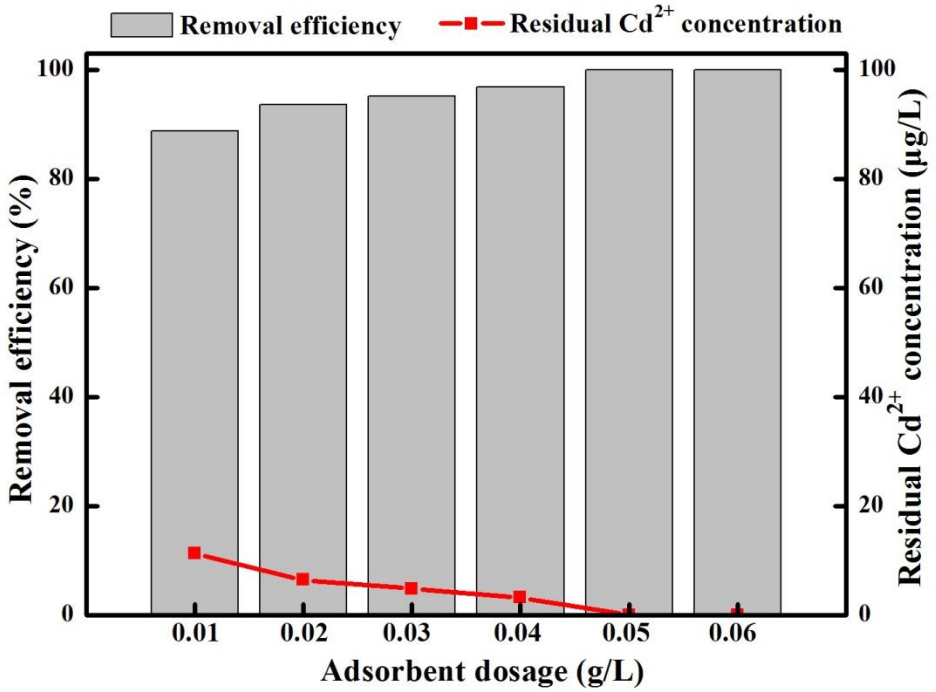

Fig. 7 Removal of trace level of Cd(II) using bentonite-Fe_3O_4-MnO_2 with different dosages

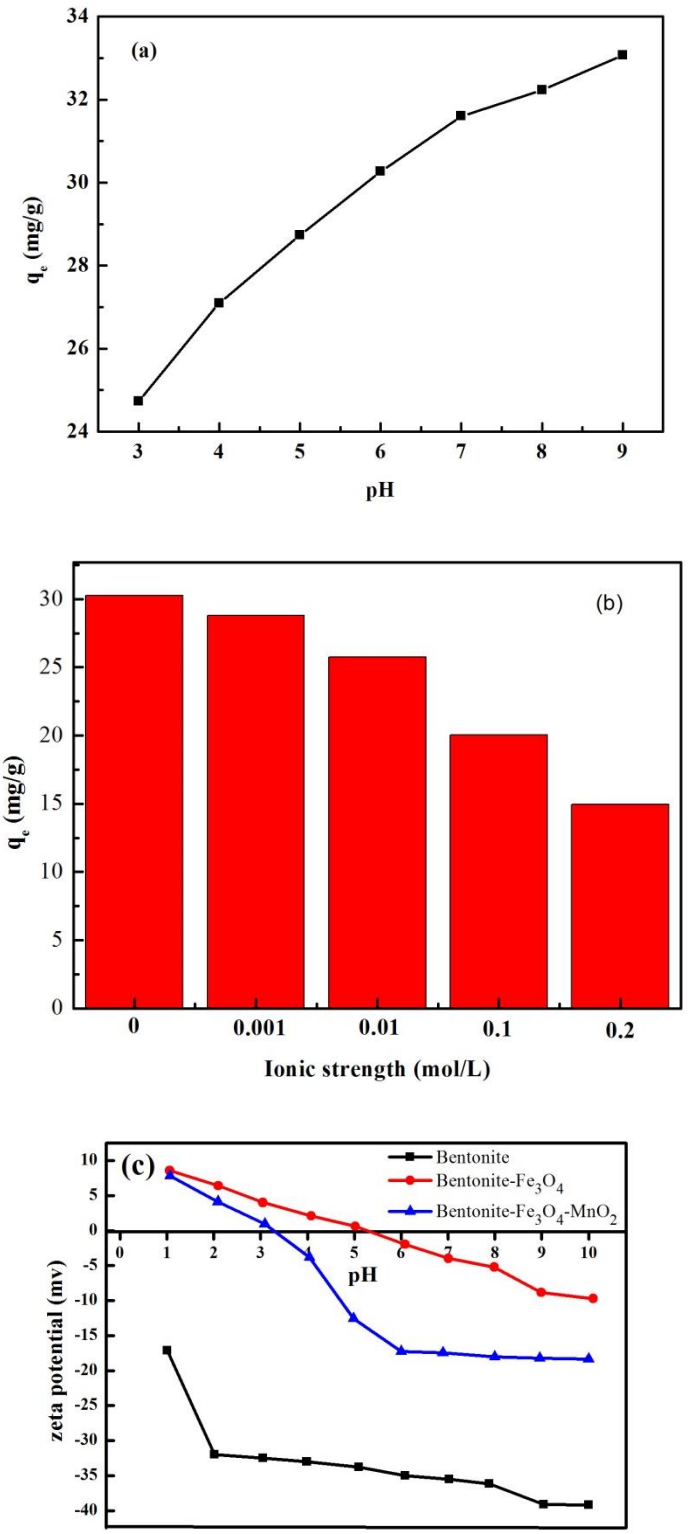

Fig. 8. Effects of pH (a) and ionic strength (b) on the adsorption of Cd(II) by bentonite-Fe_3O_4-MnO_2; and determination of pH_{PZC} of three adsorbents (c)

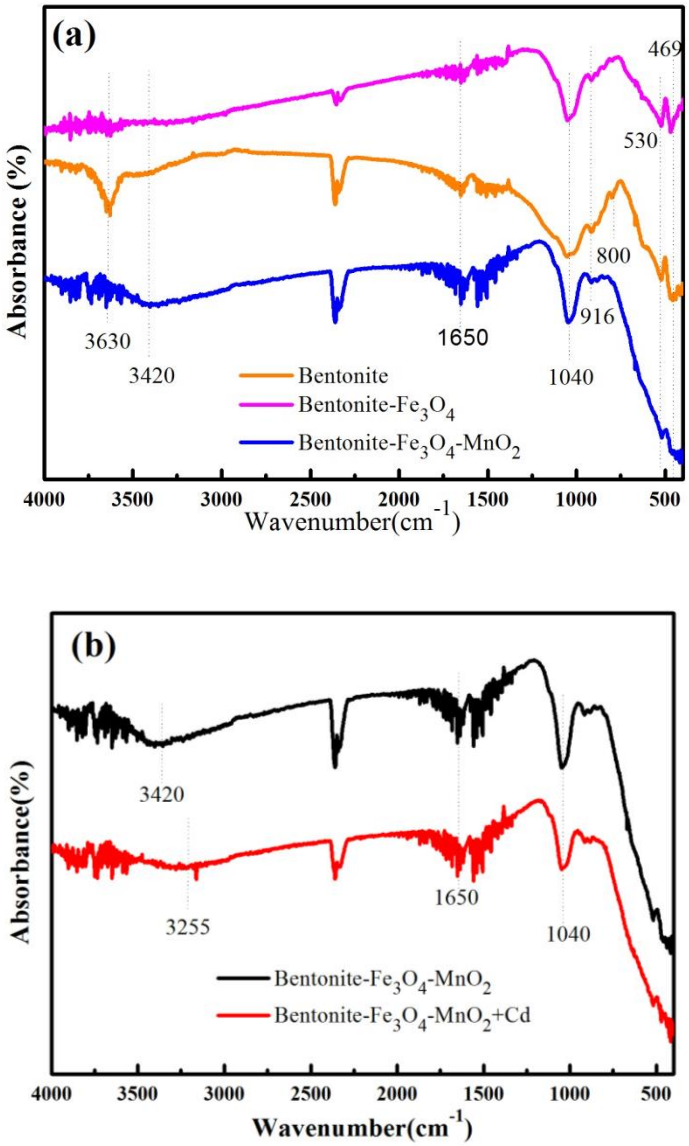

Fig. 9. The FTIR spectra of bentonite, bentonite-Fe_3O_4 and bentonite-Fe_3O_4-MnO_2 (a); The FTIR spectra of bentonite-Fe_3O_4-MnO_2 before and after reaction with Cd(II) (b)

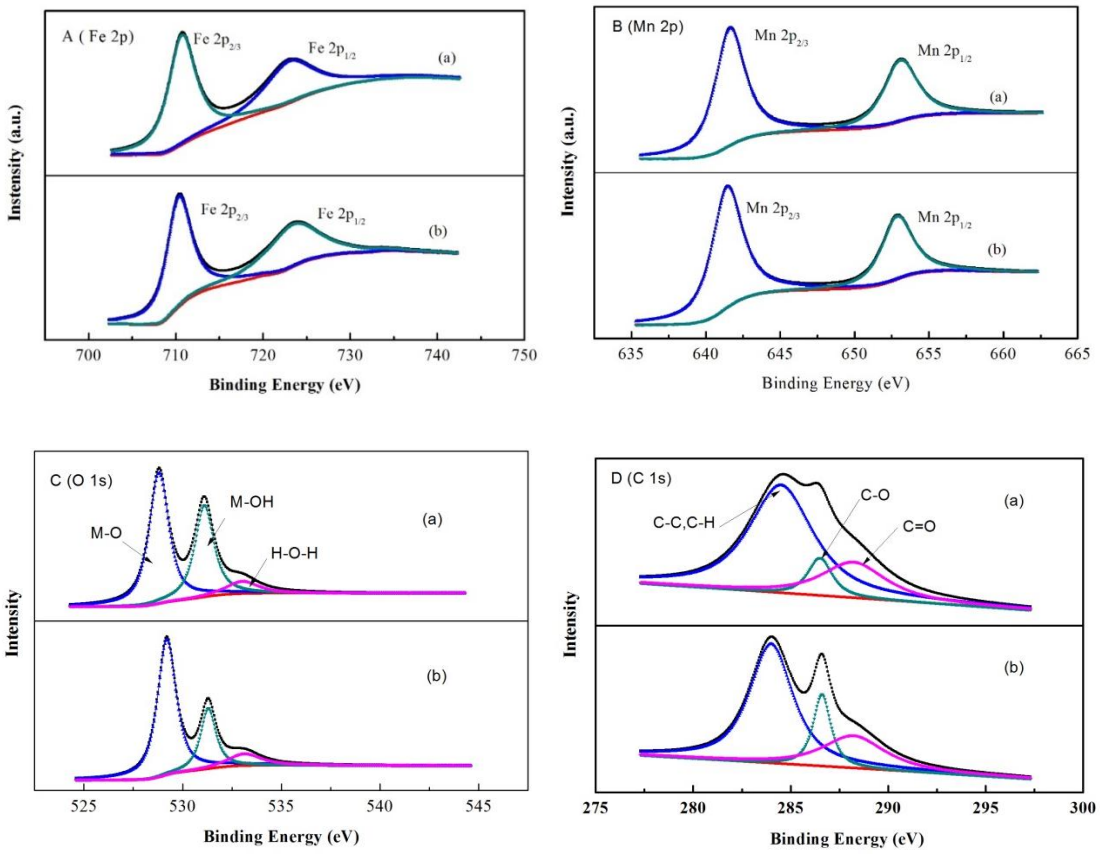

Fig. 10. Fe 2p(A), Mn 2p(B), O 1s (C) and C 1s (D) XPS spectra of bentonite-Fe_3O_4-MnO_2 (a), bentonite-Fe_3O_4-MnO_2 with Cd (II) adsorbed (b)

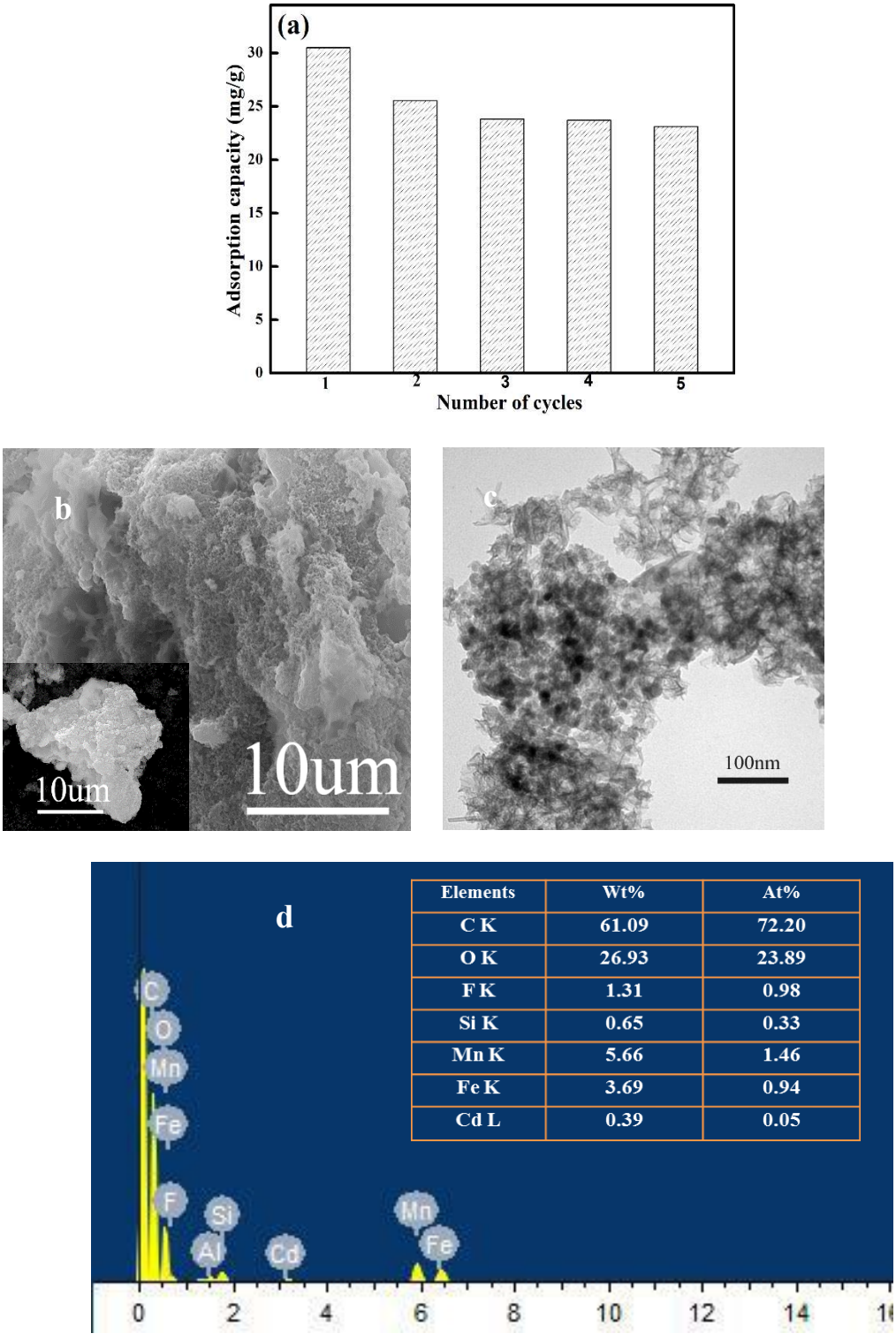

Elements	Wt%	At%
C K	61.09	72.20
O K	26.93	23.89
F K	1.31	0.98
Si K	0.65	0.33
Mn K	5.66	1.46
Fe K	3.69	0.94
Cd L	0.39	0.05

Fig. 11. Cd (II) removal by bentonite-Fe_3O_4-MnO_2 over five successive adsorption-desorption cycles (a); SEM image (b), TEM image (c) and EDX spectrum (d) of regenerated bentonite-

Fe_3O_4-MnO_2

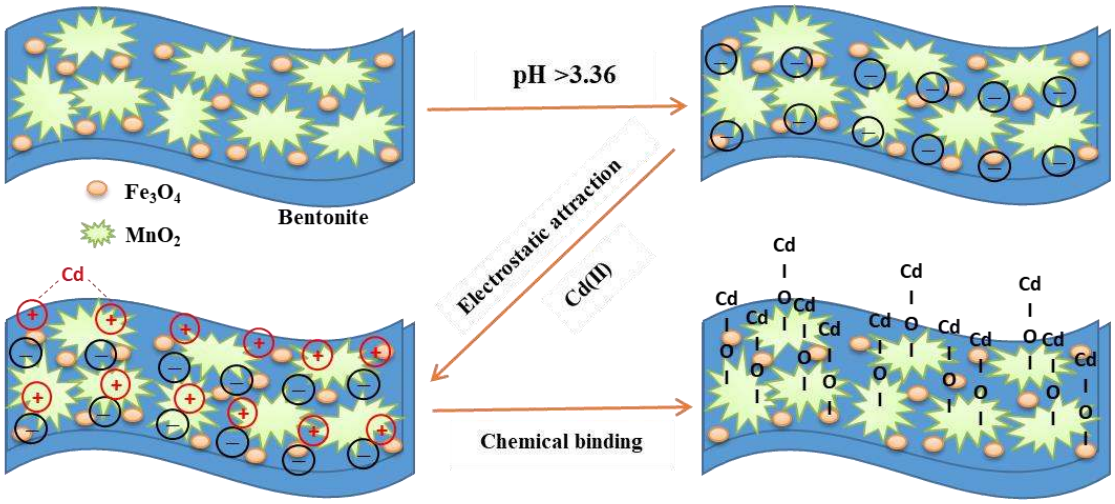

Scheme 1. Cd (II) adsorption mechanism onto bentonite-Fe_3O_4-MnO_2

Table 1. Pore parameters of bentonite, bentonite-Fe_3O_4 and bentonite-Fe_3O_4-MnO_2

Samples	S_{BET}(m^2/g)	Pore volume (cm^3/g)	Pore size (nm)
Bentonite	30.14	0.093	12.4
Bentonite-Fe_3O_4	89.25	0.28	12.7
Bentonite-Fe_3O_4-MnO_2(1:1.5)	796.99	1.70	8.5

Table 2. Parameters of two kinetics models for Cd(II) adsorption by bentonite-Fe_3O_4-MnO_2

	Experimental data	Pseudo-first-order kinetic model			Pseudo-second-order kinetic model		
	$q_{e,exp}$ (mg/g)	$q_{e,cal}$ (mg/g)	k_1 (min^{-1})	R^2	$q_{e,cal}$ (mg/g)	k_2 (min^{-1})	R^2
Bentonite	27.43	31.26	0.099	0.6857	26.94	0.068	0.9998
Bentonite-Fe_3O_4	20.93	8.21	0.231	0.8249	20.94	0.157	0.9995
Bentonite-Fe_3O_4@ MnO_2	30.17	40.20	0.156	0.9062	30.23	0.054	0.9999

Table 3. Langmuir and Freundlich adsorption isotherm parameters for Cd^{2+} adsorption onto bentonite-Fe_3O_4-MnO_2

Langmuir			Freundlich		
q_m (mg/g)	K_L (L/mg)	R^2	K_F (mg/g)	1/n	R^2
35.35	3.53	0.882	23.43	0.088	0.919